Evaluation of hydrogen embrittlement induced damages in steels using acoustic emission

Veronique Smanio, Thierry Cassagne, Francois Ropital, Jean Kittel, Marion Fregonese, Bernard Normand

EVALUATION OF HYDROGEN EMBRITTLEMENT INDUCED DAMAGES IN STEELS USING ACOUSTIC EMISSION

Véronique Smanio, Thierry Cassagne
TOTAL, ave Larribau
64018 Pau cedex – France
Email: veronique.smanio@ifp.fr

François Ropital, Jean Kittel
IFP
BP3 - 69360 Solaize – France

Marion Frégonèse, Bernard Normand
MATEIS, INSA-Lyon, CNRS UMR 5510,
69621 Villeurbanne cedex – France

ABSTRACT

In the oil and gas industry, it is known that equipments which operate in hydrogen sulfide (H_2S) media can be subjected to damages like Hydrogen Induced Cracking (HIC) and Sulfide Stress Cracking (SSC). At the present time, material selection for sour environments is generally obtained using standard tests (NACE TM0177 and NACE TM0284) which give information about the resistance of steels in sour service. These tests are suitable for a quick assessment of candidate steels by operators or steel suppliers. However they cannot provide detailed information to better understand and quantify the damage occurring during the service life of steel components.

Acoustic emission (AE) is an efficient technique to monitor degradation of materials. In the present work it is used for the early detection, characterization and time progress description of cracking phenomena caused by hydrogen embrittlement of steel in sour media.

The methodology used for the identification of AE sources related to HIC (H_2 bubbles, FeS corrosion layer, cracking) is described. AE results are discussed and correlated with crack length ratio and AE performance for quantifying HIC damage is evaluated.

Keywords: Hydrogen Induced Cracking, Acoustic Emission, hydrogen sulfide, steels.

INTRODUCTION

Steels used in presence of production waters containing H_2S can be susceptible to different types of Hydrogen Embrittlement (HE), like HIC and SSC

HIC is a planar mode of cracking that develops in carbon and low alloy steels when atomic hydrogen diffuses into the metal and then combines to form molecular hydrogen at trap sites. Crack initiation and propagation result from the pressurization of trap sites by hydrogen. No external applied stress is needed for HIC development. Trap sites involved in HIC are commonly found in steels containing a high density of planar inclusions like MnS and/or regions of anomalous microstructure (e.g. pearlitic structure) produced by segregation of impurities and alloying

elements. SSC leads to the early failure of the metal due to the combined effect of both hydrogen penetration and tensile stress (residual and/or applied) in wet H_2S environment. High strength metallic materials and hard welded zones are prone to SSC.

The present work is focused on HIC, but study of SSC by AE is one of the future prospects of the study.

The selection of HIC resistant steels is usually done with standard tests (NACE TM0284[1] or EFC 16[2] recently brought together in NACE MR0175/ISO 15156[3]) in sour media. In these tests, material damage is evaluated through cracking ratios measured in three equidistant cross-sections of the tested specimens (Crack Sensitivity Ratio, CSR, Crack Length Ratio, CLR and Crack Thickness Ratio, CTR). Information provided by these ratios is very local because it represents only the cracking state into 3 sections. Depending on the metallographic procedure used to observe cracks randomly distributed within the material, there is a marked deficiency in standard test sensitivity. Furthermore, metallographic examination is solely representative of the cracking that is achieved after the total duration of the test. Other important information is missing, e.g. the incubation time before initiation of cracking, or the evolution of cracking with time. If standard test methods are well suited for fit-for-purpose testing, they hardly give information on the mechanisms of cracking.

On the other hand, the AE technique is a non destructive evaluation method allowing the detection of active defects within materials in real time during the test. Each AE event gives rise to elastic waves which propagate into the material and results in detectable AE signals[4]. Therefore materials can spontaneously generate transient elastic waves, called AE, when they undergo solicitations. Good correlations were recently obtained between specific AE parameters and amplitude of corrosion damage in various cases: stress corrosion cracking[5-8], abrasion or erosion corrosion[9], pitting corrosion[10-13], crevice corrosion[14-15], exfoliation corrosion[16], and uniform "acidic" corrosion[17]. Among the variety of mechanisms of deformation and damage that can be sources of AE, corrosion processes take a particular position, as the acoustic source is often not the electrochemical corrosion driving force itself, but its consequence: bubble formation, crack propagation, modifications of corrosion products deposits[5-6], whether corrosion is localized or uniform.

The following corrosion reactions describe the behavior of steel immersed in an acidic media[18]:

- anodic reaction,

$$Fe \rightarrow Fe^{2+} + 2e^{-} \tag{1}$$

- cathodic reactions,

$$2H^{+} + 2e^{-} \rightarrow 2H_{ads} \rightarrow \begin{cases} (1-\varepsilon')H_2 & (2) \\ 2\varepsilon' H_{abs} & (3) \end{cases}$$

The recombination of a part of hydrogen resulting from the cathodic reaction induces hydrogen evolution (equation 2), when the other part ($\varepsilon'<1$) is absorbed inside the material (equation 3). Furthermore, in the presence of H_2S, a sulfide layer is created at the steel surface. Hydrogen uptake into the material is also enhanced by H_2S (promotion of reaction 3 or poisoning of reaction 2), leading to HE. Under these conditions, the physical phenomena potentially leading to acoustic emission are linked to:

- H_2 evolution resulting from the corrosion reaction,
- Presence of the sulfide layer on the metal surface,
- Cracking resulting from absorption, diffusion and trapping of hydrogen.

In the past, AE technique was applied to monitor hydrogen embrittlement in several studies[19-24]. Cayard et al.[19] and also Gingell et al.[20] showed that during SSC tests leading to the failure of the tested metal, a higher AE energy build-up rate was recorded compared to no-failure tests. This critical energy build-up rate associated with SSC failure remained dependant on the tested steels and the applied stress level. Weng et al.[22] found a correlation between HIC damage evaluated by CLR and the AE energy level. Moreover, Gingell et al.[20] showed that AE could be used to discriminate initiation and propagation stages of SOHIC (Stress Oriented Hydrogen Induced Cracking) development during NACE TM0177-96[25] method A tensile tests. In all these studies, AE data were treated in a global manner, i.e. considering simultaneously all the AE sources involved during the test.

In that context, the first step of the present work was to discriminate the different AE sources in order to identify the acoustic signature of HIC signals. Using this discrimination, a correlation between AE data and HIC damage amplitude was established and more information on cracking kinetics can be obtained.

EXPERIMENTAL PROCEDURE

Materials

Two API X65 grade pipeline steels were used as reference materials. One was identified as X65 Sweet Service (SwS) grade because of its poor HIC resistance and the other was identified as X65 Sour Service (SS) grade.

The chemical compositions of both X65 grade steels were analyzed by optical emission spectroscopy (OES), except for carbon and sulfur, analyzed by a chemical method (Table 1).

For microstructure observation, the specimens were ground with silicon carbide (SiC) paper down to 1200 grade and polished down to 0.05µm diamond suspension and then etched with a Nital solution (2%vol. nitric acid and ethanol). The microstructure was observed in the longitudinal transverse direction (LT) using an optical microscope. The different microstructures at the mid wall location are presented in Figures 1 and 2. The major phases observed for both steels are pearlite and ferrite. For the sour service grade, the microstructure is equiaxed and homogenous, which accounts for its good HIC resistance. The microstructure of the sweet service grade is highly oriented in the rolling direction, which explains its poor HIC resistance.

The tensile properties of both steels in the parallel to rolling direction are gathered in Table 2. The inclusion content was analyzed according to ASTM E45 method A[26]. The results are presented in Table 3. No significant difference is observed between both grades in terms of inclusion content, which confirms that the difference of HIC sensitivity between the selected steels is mainly linked to ferrite and pearlite distribution and grain orientation.

Experimental Set up

The experimental set up (Figure 3) was based on the SSC standard test NACE TM0177-96[25] device. The specimen was placed in a proof ring, but without applied load. Only the gauge section of the sample was immersed in the corrosive solution. Tests were conducted in buffered solution according to EFC 16[2] (5 wt% NaCl and 0.4% CH_3COONa in distilled water) under 1 bar H_2S. De-aeration conditions by nitrogen bubbling were studied, and a procedure of de-aeration was used to obtain less than 15 ppb dissolved oxygen. In this preliminary study, oxygen content during de-aeration was measured by an oxygen gas sensor placed in the cell. This de-aeration procedure was applied before each test.

A circulation of the corrosive fluid (sour media) was ensured between the test cell and a vessel, in which gas bubbling was maintained. This procedure allowed to avoid any interfering AE noise detection (e.g. gas bubbling in the test cell would result in AE) and to maintain constant electrochemical conditions in the cell during the test (easier pH control). The pH was measured with a pH meter located in this second vessel and adjusted every day through HCl or NaOH additions.

The AE technique was designed for this test, two AE sensors located at the top and bottom of the specimen (Figure 3) in order to detect AE signals. AE instrumentation consisted of a transducer, a preamplifier and a data acquisition system.

Methodology

The successive experimental steps that were applied for identification of acoustic signature of individual sources are summarized in Table 4. A first series of tests was conducted without H_2S under cathodic polarization in order to identify AE signals resulting from H_2 evolution. Then, a second series of tests was conducted under 1 bar H_2S at pH 4.5 on both sour service and sweet service steels to discriminate sulfide layer induced AE signals from HIC induced AE signals.
After the tests, evaluation of HIC damage was performed with four equidistant cuts along the length and metallographic examination of the faces. CLR and CSR were then calculated. However, the specimen geometry was similar to SSC tensile specimens as per NACE TM0177[25], with a 6.35 mm diameter section. This dimension is rather small compared to standard HIC specimens which are 20 mm wide. It is therefore expected that the experimental error and scattering of crack ratios determined from the small SSC shaped specimens could be significant.

RESULTS

Identification of the different AE sources

The first test batch consisted in a cathodic polarization of the X65 SS grade immersed in the test solution under 1 bar N_2 at pH 5.5. The applied current density was -280 µA/cm², corresponding approximately to a cathodic potential of -1250 mV/(Ag/AgCl). The tests lasted 8 hours. The cathodic reaction leading to H_2 evolution was enhanced by a cathodic potential to the sample; at the same time the anodic reaction resulting in iron dissolution was limited.

Under these conditions, only one AE source was active: the evolution of hydrogen gas resulting from the cathodic reaction. No HIC resulting from cathodic hydrogen charging was observed in the sour service steel. Several AE parameters were studied, AE energy and signals duration were found to be the most discriminating parameters.

Therefore, AE results are presented in a correlation chart representing the absolute energy of the signals as a function of their duration (Figure 4). On this figure, each point represents one AE event.

In order to identify the AE hits related to the sulfide layer and HIC, further tests were performed on sour service and sweet service steels at pH 4.5 under 1 bar H_2S. Cracks were only observed in the sweet service steel grade. They are localized in the bands of pearlite at mid-wall location (Figure 5).

The characteristics of the AE signals recorded during the former test (pH 4.5, 1 bar H_2S) performed on the sour service steel are presented in Figure 6. As compared with the AE diagram obtained for H_2 evolution under cathodic polarization (Figure 4), a new AE class was detected, with higher absolute energy signals. As no cracks were detected for these experimental conditions, it can be assumed that this class B was related to the presence of the sulfide layer at the sample surface.

AE results obtained during tests performed on the sweet service steel grade are presented in Figure 7. As previously, H_2 evolution and sulfide layer classes can be identified again. In addition, a third AE class exhibiting signals with higher duration was detected. Metallographic observations of the sample after the test confirmed the presence of HIC. This AE class was correlated with cracking within the material.

As a result the experimental approach was able to discriminate and identify the three main AE sources namely hydrogen evolution, iron sulfide film formation and HIC.

Correlation between HIC damage and AE data

Using the discrimination, it was then possible to separate all AE data related to HIC for one entire test. The evolution with time of HIC specific AE signals was examined for different tests.

Tests were performed on X65 SwS grade at pH 4.5 under 1 bar H_2S with different exposure time from 5 to 65 hours in order to obtain different damage level in samples. HIC damage evaluation was performed with four equidistant cuts along the length and metallographic examination of the faces. CLR and CSR ,define according to NACE TM0284[1] ,were then calculated. AE data and cracking state of samples resulting from these interrupted tests are given in Table 5.

For tests 1 to 11, only purely internal cracks, i.e. not open to surface, were detected (Figure 8). All samples exhibit a CSR ranged between 0 and 2 % whereas the CLR varies from 0 to 82 % (Table 5). Since CSR do not vary from one sample to another, CLR was chosen as a criterion for quantifying HIC damage in the considered samples (1 to 11).

Tests 12 and 13 are quite different from the other tests since open to surface cracks, and higher CSR were observed in these two samples (figure 9). Since these two samples present a different cracking behaviour, they are considered apart from the others for the correlations with AE data. At present, no explanation was found to understand the different cracking state between these two samples and the other ones.

In the past, the global AE energy recorded during the test was chosen as a criterion for detecting and quantifying the formation of cracks[19-20,22]. Weng et al.[22] observed higher global AE energy level for samples exhibiting cracks but AE was treated in a global manner i.e. considering simultaneously all the AE sources involved during the test.

In this study, signals related to HIC were clearly identified so that these signals can be now isolated from all other AE signals. Thus, the evolution of either global cumulative acoustic energy or only HIC class cumulative energy for tests 1 to 11 as a function of the CLR calculated was drawn (Figure 10). No direct correlation was found

between the AE global energy detected during the test (i.e. considering all the AE sources) and the damage amplitude represented by the CLR. On the other hand, a good correlation is obtained between CLR and AE cumulative energy related to HIC signals only (Figure 10). The discrimination of HIC AE events allows therefore a direct correlation with cracking extent, using CLR. The latter is the most relevant parameter because in the Sweet Service steel all cracks are located in the mid section area.

Using the same discrimination of AE sources, the evolution with time of HIC related AE was then examined (Figure 11) for tests 1 to 11. Even though some scattering is observed, probably due to the intrinsic scattering of defect areas in the small section specimens, all curves present similar trends, with three successive stages:

- an initial period with hardly no AE related to HIC,
- a step increase of AE related to HIC,
- a final period with hardly no AE related to HIC.

The initiation period varies from 1 hour in specimen 7 to 25 hours in specimen 5 which could correspond to the time necessary for adsorbed hydrogen to diffuse and to be trapped within the material and generate cracking.
The curves indicate that the high energy step corresponds to the crack propagation and lasts from 2 to 20 hours depending on the test. Then, it can be observed that HIC propagation stops.

AE measurements give therefore real time information about the incubation time and the propagation period required for HIC.

As mentioned previously, because cracks in samples 12 and 13 are reaching the outer surface tests 12 and 13 cannot be directly compared to the others (Figure 9). At the same time, higher AE cumulative energy related to HIC were recorded for these tests. Cracks opening at the sample surface give rise to higher AE energy even if opened cracks are shorter than purely internal ones. At present, not enough samples presenting this cracking state were observed to establish a clear correlation between AE data and HIC damage. AE energy due to HIC is linked to the cracking state of the sample and improvement is expected by a better 3D quantification of HIC damage in the sample. This might be achieved by non destructive methods, such as ultrasonic inspection or X-ray tomography. Both techniques are being used and compared in order to obtain a better assessment of cracking in the specimens.

CONCLUSIONS

AE monitoring was carried out during standard tests devoted to characterize sensitivity of steels in sour environment.

The first step of the study consisted in discriminating the AE signature of HIC from other sources, such as hydrogen evolution and formation and/or cracking of the iron sulfide layer. This was achieved by a series of tests, and a good discrimination of the different sources was found from the energy and duration of each acoustic event. For a given sour service test, it was then possible to separate the AE related to HIC from all other sources. This gives a much better signal to noise ratio when evaluating HIC, as compared to previous works using all AE data with no filtering.

Using the sole AE data related to HIC, the method was used then to study both kinetic and cracking extent.

It was found that the cumulative energy of AE related to HIC correlates well with HIC damage level. A good correlation was obtained between this energy and the CLR for different samples presenting low CSR and purely internal cracks. Higher CSR and open to surface cracks seems to induce higher AE energy level. This correlation is then probably highly specific to one material and one crack mechanism.

Furthermore, the identification of HIC signals also allows to study the kinetics of HIC. It was clear that HIC exhibited an incubation period, followed by the initiation and propagation of cracks, until the maximum damage was reached. Such data in mildly sour conditions would be extremely useful: indeed, the minimum test duration for HIC fit-for purpose tests in mildly sour conditions is still a topical question[27]. With that aim, some tests in the specific nodes of the pH – pH_2S severity diagram could help for a better understanding of HIC mechanisms.

In the future, a parallel methodology will be applied to SSC.

REFERENCES

1. NACE International Standard Test Method NACE TM0284-96, Evaluation of pipeline and pressure vessel steels for resistance to Hydrogen Induced Cracking, NACE, 1996
2. S. Eliassen, L. Smith, P. Jackman, Guidelines on materials requirements for carbon and low alloy steels for H_2S-containing environments, Oil and gas production 2nd Edition European Federation of Corrosion (EFC number16), 2002
3. NACE MR0175/ISO 15156-2, Petroleum and natural gas industries - Materials for use in H_2S containing environments in oil and gas production - Part 2: Cracking-resistant carbon and low alloy steel, and the use of cast iron, 2003
4. Roget J., Essais non destructifs, l'émission acoustique: mise en oeuvre et applications, AFNOR et CETIM ISBN 2122690119
5. H. Mazille, R. Rothéa The use of acoustic emission for the study and monitoring of localized corrosion phenomena, Tretheway KR, Roberge PR, editors. Modeling aqueous corrosion, Netherlands: Kluwer Academic, 1994, pp 103-127
6. S. Yuyama, T. Kishi and Y. Hisamatsu, AE Analysis during Corrosion Cracking and Corrosion Fatigue Process, Journal of Acoustic Emission, 1983, vol.2, n°1/2, pp 71-93
7. W. J. Pollock, D. Hardie and N. J. H. Holroyd, Monitoring Sub-Critical Crack Growth due to Stress Corrosion or Hydrogen Embrittlement by Acoustic Emission, British Corrosion Journal, 1982, vol.17, n° 3, pp 103-111
8. W. W. Gerberich, R. H. Jones, M. A. Friesel and N. Nozue, Acoustic Emission Monitoring of Stress Corrosion Cracking, Materials Science and Engineering,1988, vol.103, pp 185-191
9. F. Ferrer, H. Idrissi, H. Mazille, P. Fleischmann, P. Labeeuw, On the potential of acoustic emission for the characterization and understanding of mechanical damaging during corrosion-abrasion processes, Wear, 1999, vol.231, pp 108-115
10. R. H. Jones and M. A. Friesel, Acoustic Emission during Pitting and Transgranular Crack Initiation in Type 304 Stainless Steel, Corrosion, 1992, vol.48, n° 9, pp 751-758
11. H. Mazille, R. Rothea, C. Tronel, An Acoustic emission Technique for Monitoring Pitting Corrosion of Austenitic Stainless Steels, Corrosion Science, 1995, vol.37, n° 9, pp 1365-1375
12. M. Fregonese, H. Idrissi, H. Mazille, L. Renaud and Y. Cêtre, Monitoring Pitting Corrosion of AISI 316L austenitic stainless steel by acoustic emission technique: choice of Representative Acoustic parameters, Journal of Materials Science, 2001, vol.36, pp 557-563.
13. M. Fregonese, H. Idrissi, H. Mazille, L. Renaud and Y. Cetre, Initiation and propagation steps in

pitting corrosion of austenitic stainless steels: monitoring by acoustic emission, Corrosion Science, 2001, vol.43, n°4, pp 627-641
14. Y.P. Kim, M. Fregonese, H. Mazille, D. Féron, G. Santarini, Ability of acoustic emission technique for detection and monitoring of crevice corrosion on 304L stainless steel, NDT&E International, 2003, vol.36, pp 553-562
15. Y.P. Kim, M. Fregonese, H. Mazille, D. Féron, G. Santarini, Study of oxygen reduction on stainless steel surfaces and its contribution to acoustic emission recorded during corrosion processes, Corrosion Science, 2006, vol.48, n°12, pp 3945-3959
16. F. Bellanger, H. Mazille, H. Idrissi, Use of acoustic emission technique for the early detection of aluminum alloys exfoliation corrosion, NDT&E International, 2002, vol.35, pp 385-392
17. L. Jaubert, M. Fregonese, D. Caron, F. Ferrer, C. Franck, E. Gravy, P. Labeeuw, H. Mazille, L.Renaud, On the opportunity to use non-intrusive acoustic emission recordings for monitoring uniform corrosion of carbon steel and austenitic stainless steel in acid and neutral solutions, Insight, 2005, vol.47, n°8, pp 465-471
18. Jacques Galland, Jaroslav Sojka, Michel Jérome. Chapitre 12: Introduction d'hydrogène dans les aciers. Dans Prévention et lutte contre la corrosion publié sous la direction de Bernard Normand, Nadine Pébère, Caroline Richard et Marine Wery, Presses polytechniques et Universitaires Romandes, Coll. INSA de Lyon, Lausanne, p273, 2004.
19. M.S. Cayard, R.D. Kane, Evaluation of various methods of reducing the duration of SSC qualification testing, Corrosion 97, paper n°57
20. A.D.B. Gingell, X.Garat, Observations of damage modes as a function of microstructure during NACE TM0177-96 tensile testing of API 5L grade X60 linepipe steel, NACE International, 1999, paper n°600
21. C-C. Weng, R-T. Chen, Acoustic emission characterization of steel in H_2S solution subjected to tensile load, Journal of Chinese Institute of Engineers, 1993, vol.16, n°4, pp 489-498
22. C-C. Weng, R-T. Chen, Acoustic emission characteristics of a high-strength steel subjected to corrosive hydrogen sulfide solution, Journal of the Chinese Institute of Engineers, 1993, vol.16, n°2, pp 195-202
23. S.Y. Tsai et H.C. Shih, Correlation between acoustic emission signals and hydrogen permeation in high-strength, low alloy steel cracking in wet H_2S, Journal of the Electrochemical Society, 1998, vol.145, n°6, pp1968-1976
24. S. Amami, P. Marchand, S. Duval, X. Longaygue, M. Fregonese, H. Mazille, J.P. Millet, Early detection and monitoring of sulfide stress cracking (SSC) of steels by an acoustic emission method, Environmental Degradation of Engineering Materials, Bordeaux, France, 2003
25. NACE International Standard Test Method NACE TM0177-96, Laboratory testing of metals for resistance to specifics forms of environmental cracking in H_2S environments, NACE, 1996
26. ASTM International, Standard test methods for determining the inclusion content of steel, ASTM, 2002
27. J.W. Martin, J. Kittel, T. Cassagne, C. Bosch, Hydrogen Induced Cracking (HIC) – Laboratory testing assessment of low allow steel linepipe, Corrosion 2008.

TABLE 1

CHEMICAL COMPOSITION (WT %) OF X65 SOUR SERVICE AND SWEET SERVICE GRADES

Steel	C	Mn	Si	P	S	Cr	Ni	Mo	Cu	Al	Ti	Nb
X65 SS	0.046	1.36	0.322	0.008	0.001	0.041	0.036	0.008	0.047	0.036	0.019	0.045
X65 SwS	0.09	1.56	0.28	0.014	0.001	0.05	0.03	0.01	0.02	0.030	0.000	0.040

TABLE 2

MECHANICAL PROPERTIES OF X65 SOUR SERVICE AND SWEET SERVICE GRADES (TESTS CONDUCTED ACCORDING TO EN10002-1 STANDARD)

Steel	$Rp_{0,2}$ ±2%	Rm ± 1.5%	A% ±2.5%
X65 SS	529 MPa	571 MPa	47
X65 SwS	523 MPa	649 MPa	24

TABLE 3

COMPARISON OF INCLUSION CONTENT OF TESTED STEELS, ACCORDING TO ASTM E45 METHOD A

Steel	Type A (sulfides)		Type B (aluminates)		Type C (silicates)		Type D (oxides)	
	Thin	Heavy	Thin	Heavy	Thin	Heavy	Thin	Heavy
X65 SS	0	0	0	2	0	0	0.5	0.5
X65 SwS	0	0	0	0	0	0	0.5	0.5

TABLE 4

ACTIVE ACOUSTIC EMISSION SOURCES AS A FUNCTION OF EXPERIMENTAL CONDITIONS AND TESTED MATERIALS

Experimental conditions				**Acoustic emission sources**		
Gas (1 atm)	pH	Steel	Polarization	H_2 evolution	Sulfide layer	HIC
N_2	5.5	X65 SS	cathodic	X	-	-
H_2S	4.5	X65 SS	no	X	X	-
H_2S	4.5	X65 SwS	no	X	X	X

TABLE 5 RESULTS OF INTERRUPTED TESTS

Test	Duration (h)	Global AE energy (10^{-18} J)	HIC class AE energy (10^{-18} J)	CLR (%)	CSR (%)	Open to surface cracks
1	25	3.6×10^{5}	2.0×10^{4}	12	0	no
2	18	1.2×10^{6}	6.5×10^{3}	2	0	no
3	18	6.5×10^{5}	1.5×10^{4}	8	0	no
4	65	2.4×10^{6}	2.9×10^{5}	82	2	no
5	65	1.2×10^{6}	3.4×10^{5}	75	2	no
6	5	1.2×10^{5}	2.0×10^{2}	1	0	no
7	5	7.0×10^{5}	1.5×10^{5}	38	0	no
8	9	1.1×10^{5}	2.4×10^{4}	1	0	no
9	9	1.9×10^{5}	3.2×10^{3}	10	0	no
10	24	5.0×10^{4}	2.4×10^{1}	0	0	no
11	46	4.7×10^{5}	1.8×10^{4}	4	0	no
12	24	3.5×10^{6}	7.4×10^{5}	57	4	yes
13	46	1.6×10^{7}	8.2×10^{6}	62	6	yes

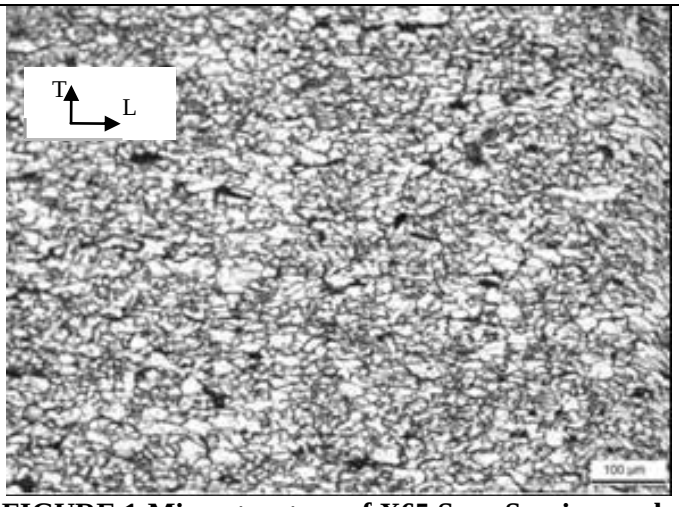

FIGURE 1-Microstructure of X65 Sour Service grade (LT plane)

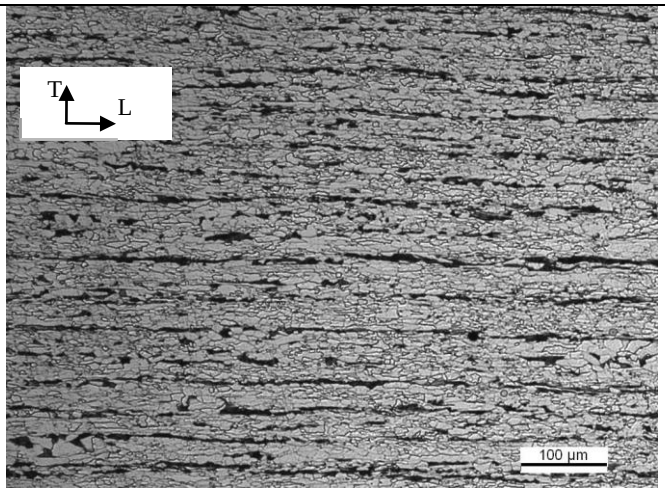

FIGURE 2-Microstructure of X65 Sweet Service grade (LT plane)

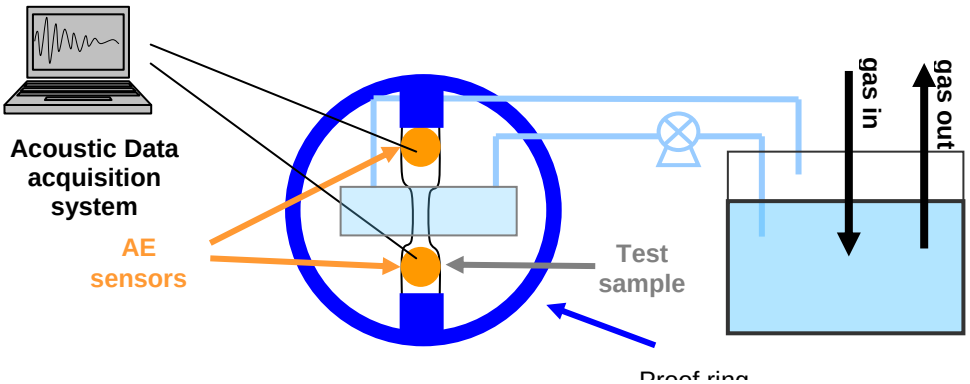

FIGURE 3-Experimental set up

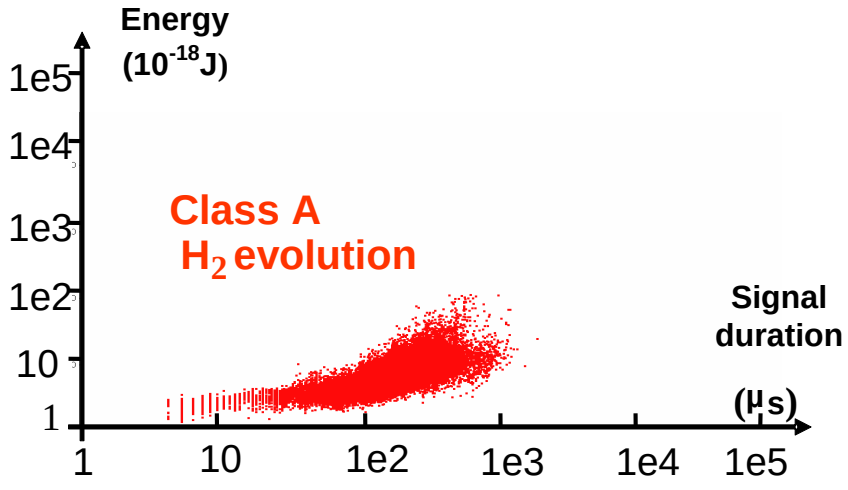

Figure 4-Correlation chart representing absolute energy as a function of signals duration for a test conducted in the EFC 16 solution at pH 4.5 under 1 bar H_2S, on a X65 SS specimen.

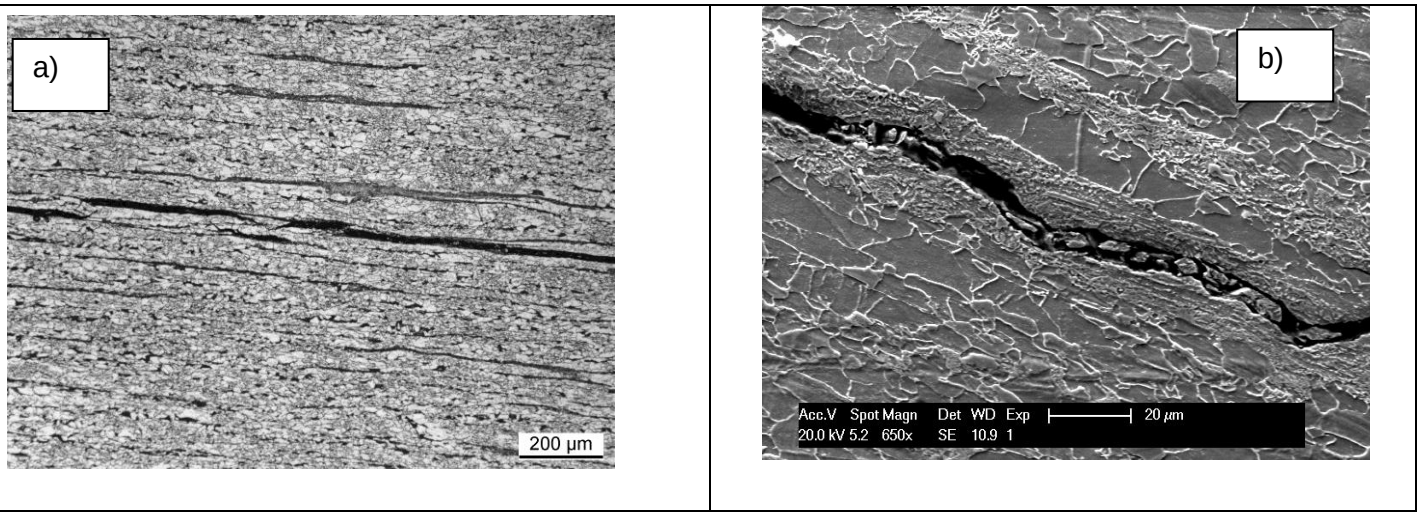

Figure 5 - HIC detected in X65 SwS after a test performed in EFC 16 solution at pH 4.5 under 1bar H_2S a) metallographic observations, b) SEM observations

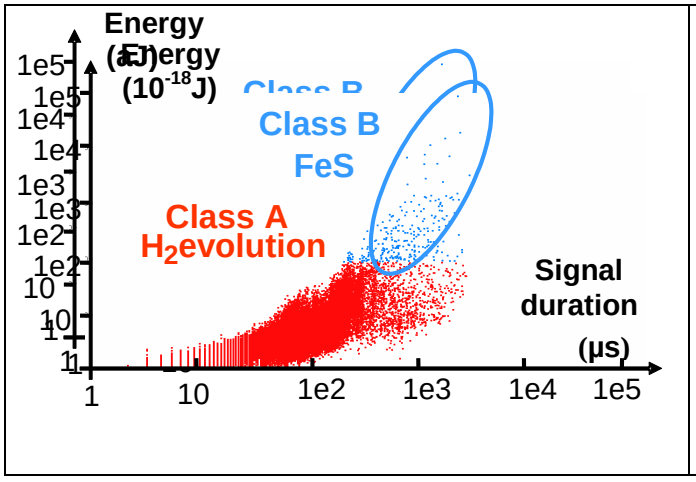

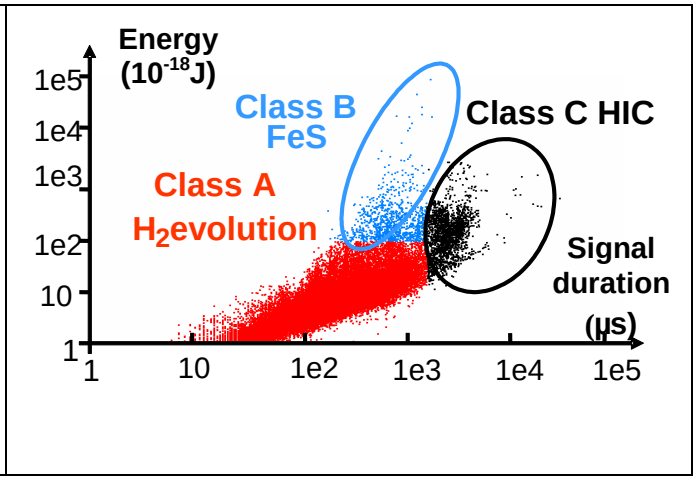

FIGURE 6 - Correlation chart representing absolute energy as a function of signals duration for a test conducted in the EFC 16 solution at pH 4.5 under 1bar H_2S on a X65 SS specimen.

FIGURE 7 - Correlation chart representing absolute energy as a function of signals duration for a test conducted in the EFC 16 solution at pH 4.5 under 1bar H_2S on a X65 SwS specimen.

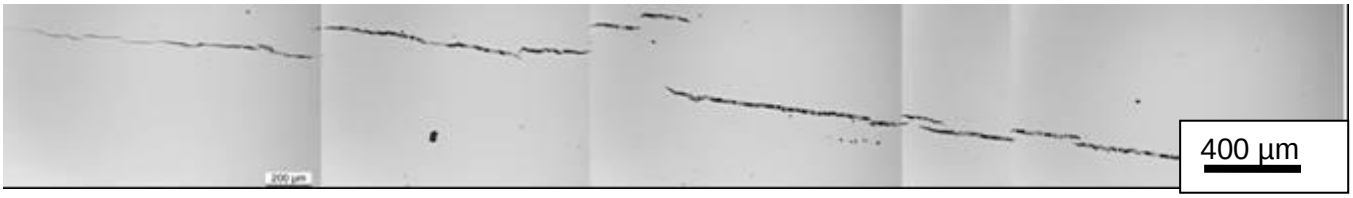

Figure 8 HIC detected in X65 SwS after the test n°4 performed in EFC 16 solution at pH 4.5 under 1 bar H_2S during 65 hours: internal cracks

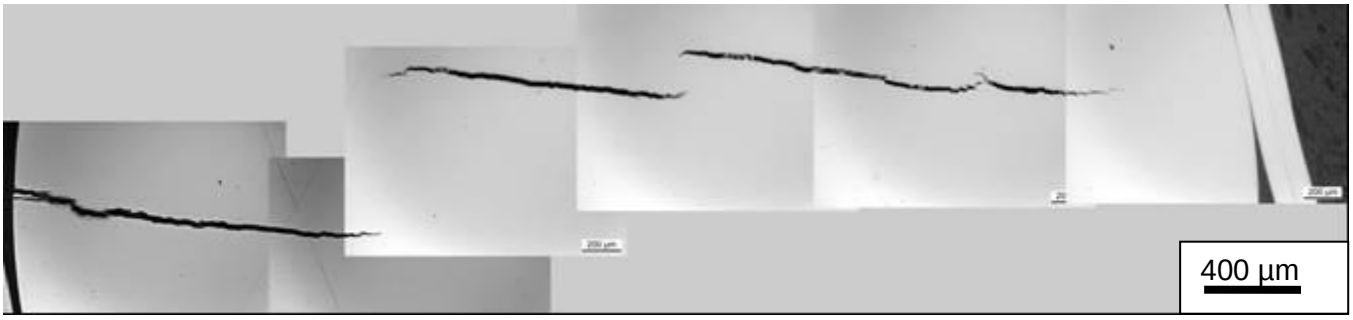

Figure 9 HIC detected in X65 SwS after the test n°13 performed in EFC 16 solution at pH 4.5 under 1 bar H_2S during 46 hours: open to surface cracks

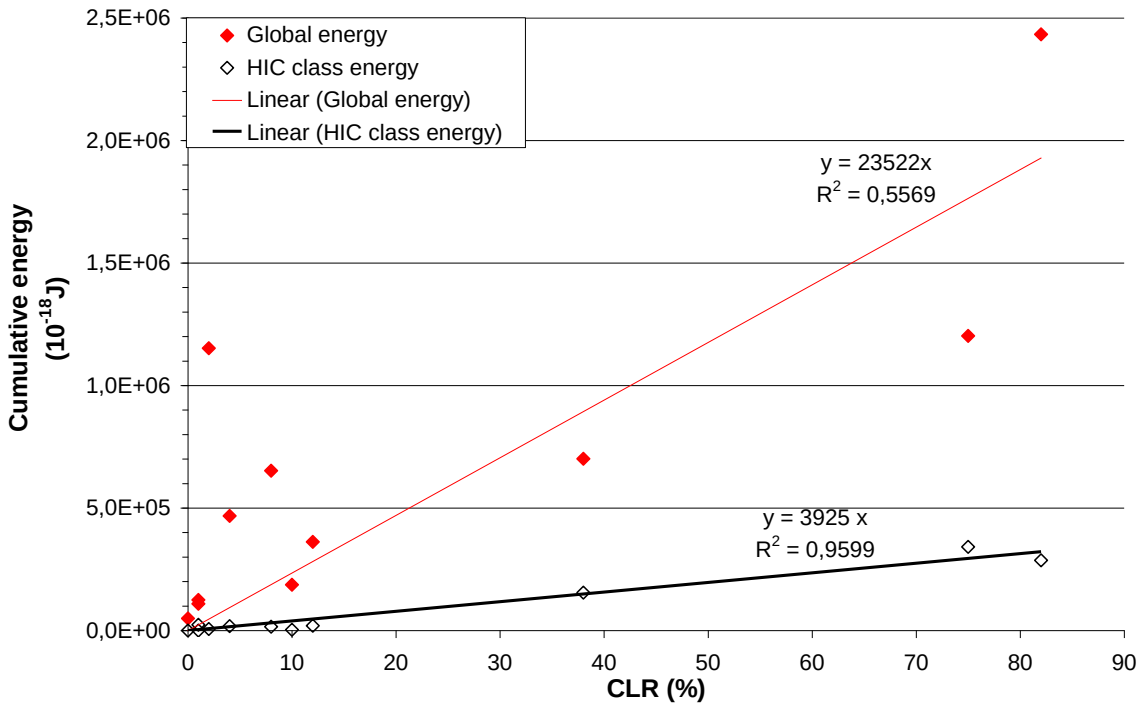

Figure 10 – Correlation graph between global (closed marks) and HIC (open marks) cumulative energy as a function of CLR for X65 Sweet Service samples tested at pH 4.5 under 1 bar H_2S for various immersion time

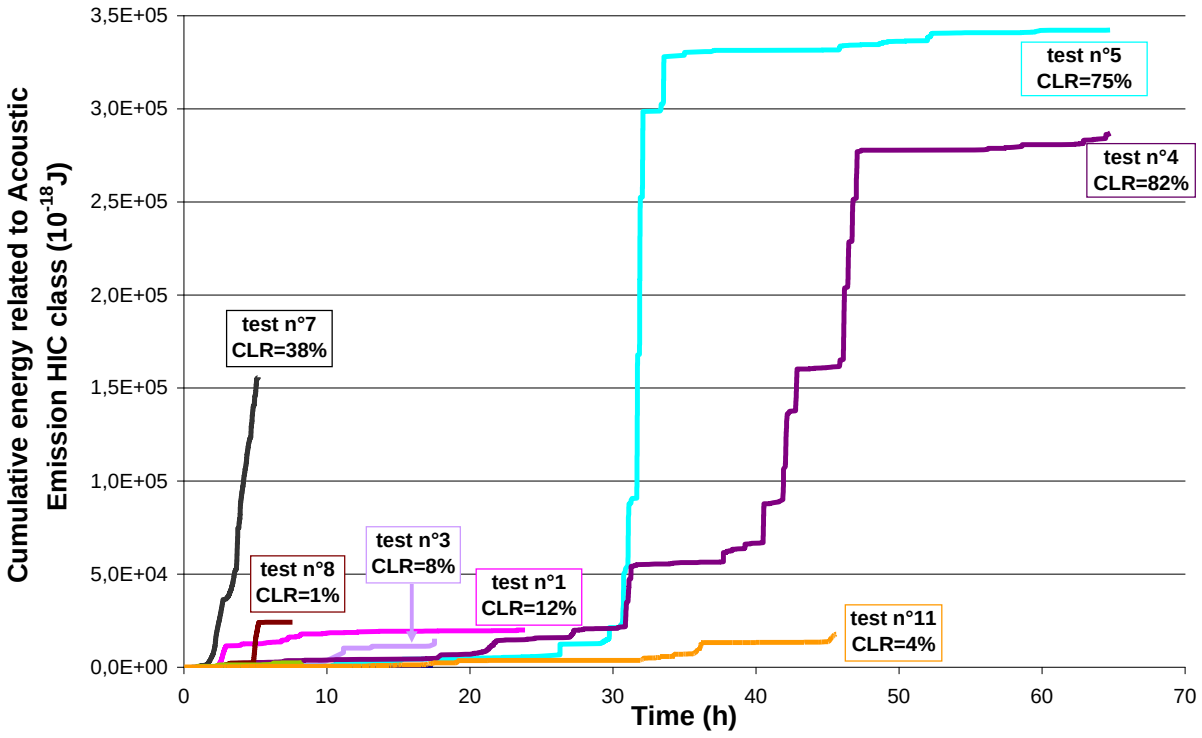

Figure 11 Evolution of cumulative energy related to HIC during the different interrupted tests (1-11)